



LAWRENCE
LIVERMORE
NATIONAL
LABORATORY

Relationship between void- and contact normal-based fabric tensors for 2D idealized granular materials

P. Fu, Y. F. Dafalias

April 10, 2014

International Journal of Solids and Structures

Disclaimer

This document was prepared as an account of work sponsored by an agency of the United States government. Neither the United States government nor Lawrence Livermore National Security, LLC, nor any of their employees makes any warranty, expressed or implied, or assumes any legal liability or responsibility for the accuracy, completeness, or usefulness of any information, apparatus, product, or process disclosed, or represents that its use would not infringe privately owned rights. Reference herein to any specific commercial product, process, or service by trade name, trademark, manufacturer, or otherwise does not necessarily constitute or imply its endorsement, recommendation, or favoring by the United States government or Lawrence Livermore National Security, LLC. The views and opinions of authors expressed herein do not necessarily state or reflect those of the United States government or Lawrence Livermore National Security, LLC, and shall not be used for advertising or product endorsement purposes.

Relationship between different fabric tensors for granular materials

Pengcheng Fu^a, Yannis F. Dafalias^{bc}

^aAtmospheric, Earth, and Energy Division, Lawrence Livermore National Laboratory, 7000 East Avenue, L-286, Livermore, CA 94551, USA
Corresponding author; Email: fu4@llnl.gov. Tel: 1-925-422-3579

^bDepartment of Civil and Environmental Engineering, University of California, Davis, CA 95616, USA

^cDepartment of Mechanics, School of Applied Mathematical and Physical Sciences, National Technical University of Athens, Athens, 15773, Greece.

Abstract:

Fabric tensors are commonly used in the study of granular materials as internal variables to quantify anisotropic fabrics. Fabric tensors can be constructed based on different microstructural entities in the material, such as particle long axis orientations, inter-particle contact normal directions, and orientations of void shapes. The current study explores the relationship between these different fabric tensors. Using two-dimensional discrete element method (DEM) simulations, we discover a simple and strong linear correlation between contact normal- and void vector-based fabric tensors for granular materials composed of non-elongated particles. This correlation holds true independent of the variations of all parameters and conditions exhaustively considered in this study, including the material's packing density, stress state, inter-particle friction angle, particle size distribution, and particle shape. For materials consisting of significantly elongated particles, the relationship between the three fabric tensors is complicated. The change of void vector-based fabric tensor's normal components appears to be positively affected by the corresponding components of the other two fabric tensors, whereas particle-based fabric tensor and contact normal-based fabric tensor tend to be negatively correlated.

Keywords: fabric tensor, anisotropic fabric, granular materials, discrete element method

1. Introduction

Fabric, a generic term in the study of granular materials mechanics, refers to characteristics of microstructure of these materials at the grain-scale. A *fabric tensor* is a metric that quantifies microstructural orientation-related characteristics of the material in a tensorial form. Based on the well-known scale interaction in mechanics, the macroscopic mechanical and hydrological behaviors of granular materials are governed by grain-scale structural characteristics and processes. Therefore, the concept of fabric is playing increasingly important roles in the understanding and modeling of granular materials' behavior. The rapid advancements of high-resolution nondestructive imaging technologies, such as x-ray computed tomography (e.g. Andò et al., 2012; Alshibli et al., 2013), and particle-based numerical simulation techniques, such as the discrete element method (Cundall and Strack, 1979; Fu and Dafalias, 2011a, 2011b; Guo and Zhao, 2013), provide unprecedented opportunities for directly observing and quantitatively measuring grain-scale features and processes. A number of constitutive models for soils have included various fabric scalar and tensor-valued entities as state variables (Dafalias and Manzari, 2004; Dafalias et al., 2004; Stallebrass and Baudet, 2004; Li and Dafalias, 2012). This reflects

an emerging trend in geomechanics research to push constitutive modeling from the purely phenomenological end towards the physics-based end along the modeling philosophy spectrum. Nevertheless, revealing microstructural mechanisms that dictate mechanical behaviors and identifying effective mathematical descriptions of particle-scale characteristics are ongoing endeavors. As elaborated below, numerous forms of fabric metrics, particularly fabric tensors have been developed to quantify granular material fabrics. The majority of them are based on three classes of microstructural features: particle orientations, inter-particle contact normal directions, and orientations of void shapes by means of properly defined void vectors. For definitiveness the corresponding tensors will be called henceforth for abbreviation particle orientation, contact normal and void vector fabric tensors, correspondingly. Most soil fabric-related studies in the literature investigate the relationship between material mechanical behavior and a specific form of fabric measurement (e.g. Cowin, 1985), whereas the relationship between different fabric quantifications, especially between those based on different classes of microstructural features, has rarely been studied.

In the current paper, we explore the relationship between fabric tensors based on different microstructural entities. Section 2 provides an extended overview, including some historical perspectives, of the various types of fabric tensors that have been proposed in the literature, as well as their intrinsic relationships with general geomechanics research. Section 3 reiterates a void vector fabric tensor definition proposed by Li and Li (2009) and formulates a slightly modified variant of the original definition, which is used as the basis for the subsequent analysis. Since the quantitative relationship between different fabric tensors cannot be analytically derived, the strategy is to test their correlations under a wide variety of conditions, as elaborated in section 4. A very strong correlation is established between the contact normal and void vector fabric tensors for materials consisting of non-elongated particles under all conditions tested. The relationship between all three classes of fabric tensors for substantially elongated particles is briefly discussed in section 5. The theoretical and practical implications of this newly discovered equivalence based on the strong correlations found, is discussed at the end.

The quantitative results used in the current paper were obtained from simulations using a discrete element code, PPDEM (Polyarc Parallel-processing Discrete Element Modeling) (Fu et al., 2012), which allows particles of a great variety of shapes to be simulated within the same framework.

2. Overview of fabric tensors proposed in the literature

2.1 General definition of fabric tensor

The most traditional variable for quantifying granular material microstructural characteristics is probably the void ratio, or interchangeably, porosity, both of which are scalars. When the anisotropy in soil fabric became a subject of research, mathematical quantities that are capable of describing direction-dependent features were required to characterize microstructural characteristics related to fabric anisotropy. In many studies reported in the literature, especially the early pioneering studies, direction-dependent microstructural features were often directly presented using histograms, in which the distribution of relative frequencies of features along different spatial orientations was plotted (Oda, 1972a, 1972b). Whereas such graphical representations are very illustrative, it is highly desirable to extract the most

essential information in the distribution and present it in a mathematically descriptive form. Fabric tensors seem to be a natural choice for this purpose, since many concepts in constitutive theories are expressed in tensorial forms.

The most widely used form of fabric tensors follows the definition developed independently but almost concurrently by Satake (1982) and Oda (1982). It has an integration form complying with continuum mechanics conventions and a corresponding summation form for dealing with discrete quantity measurements in granular materials. The integration form in the three-dimensional (3D) space reads

$$\mathbf{F} = \oint_{\Omega} E(\mathbf{n})\mathbf{n} \otimes \mathbf{n} d\Omega \quad (1)$$

where \mathbf{F} is the second-order fabric tensor; \mathbf{n} is a unit vector representing the direction of certain microstructural *entity*, for instance contact normal or the long axis of a particle; $E(\mathbf{n})$ is the directional probability density function (PDF) of this selected entity; \otimes denotes tensor product; and the integration is performed over the entire surface Ω of a unit sphere. $E(\mathbf{n})$ must satisfy

$$\oint_{\Omega} E(\mathbf{n})d\Omega = 1 \quad (2)$$

so that the trace of the obtained fabric tensor is unity. The corresponding summation form is

$$\mathbf{F} = \frac{1}{N} \sum_{a=1}^N \mathbf{n}^a \otimes \mathbf{n}^a \quad (3)$$

where N is the number of the entity being quantified in the domain; and the superscript a denotes the a^{th} entity in the assembly. The equivalence between the integration form and the summation form is evident as $E(\mathbf{n})d\Omega$ can be estimated by dividing the number of the features within $d\Omega$ by the total number. If the entity being quantified is symmetrical, i.e. an entity denoted by \mathbf{n} is identical to an entity denoted by $-\mathbf{n}$, each entity in the particle assembly is usually counted twice, as \mathbf{n} and $-\mathbf{n}$ respectively, in which case the $2N$ substitutes for N . The formulation is the same regardless which microstructural feature is being quantified. In the current paper we use the subscripts p , n , and v to represent fabric tensors based on particle orientations, contact normal directions, and void vectors, respectively.

The above definition addresses only the direction of the microstructural entities being measured. It is sometimes desirable to include additional characteristics of these entities in the measurement. For instance, the orientation of a large particle is likely to play a greater role than that of a small particle in determining the anisotropy of material properties, or the normal direction of a contact carrying greater force might be more important than that of a contact carrying less force (in the latter case the fabric tensor will not be only a purely geometrical entity). To consider these effects, we can “weight” the directional measurement by a scalar-valued characteristic l of the microstructural entity representing quantities such as particle size or contact force magnitude. The definition of the weighted fabric tensor in its continuum and discrete form is, therefore,

$$\mathbf{F} = \int_{\Omega} l E(\mathbf{n}, l)\mathbf{n} \otimes \mathbf{n} d\Omega dl = \frac{1}{N} \sum_{a=1}^N l^a \mathbf{n}^a \otimes \mathbf{n}^a \quad (4)$$

where $E(\mathbf{n}, l)$ is the joint probability density function for \mathbf{n} and l . Generally \mathbf{n} and l are not independent variables, so $E(\mathbf{n}, l)$ cannot be replaced by $E_1(\mathbf{n})E_2(l)$.

The weighted fabric tensor as calculated by equation (4) does not automatically have a unity trace, but it is trivial to normalize the obtained tensor. Weighted fabric tensors have been occasionally reported in the literature (e.g. Madadi et al., 2004) but their uses are not extensive. With the general definition presented above, different fabric tensors can be constructed by simply choosing the microstructural feature to be characterized and the scalar quantity to weight the tensor with.

2.2 Statistical interpretation of fabric tensors

The main purpose of fabric tensors as defined above, is to quantify the directional distribution of microstructural characteristics in a concise fashion that is convenient to use in constitutive modeling. For any given directional PDF of a microstructural feature, a fabric tensor can be uniquely calculated. On the other hand, a given fabric tensor does not map to a unique directional distribution. A number of methods have been proposed to map a fabric tensor to a directional PDF, for instance by Satake (1982), Oda et al. (1985), and Rothenburg and Bathurst (1992).

In the 2D space where most of the applications of fabric tensors have been reported, a unity-trace symmetrical second-order tensor has two degrees of freedom. It can be uniquely determined by two scalar values, such as the major principal direction measured by the angle $\bar{\theta}$, and the difference between the two principal components $\alpha = F_I - F_{II}$. $\bar{\theta}$ can be interpreted as the mean or predominant direction of the vector features being quantified, and α quantifies the intensity of anisotropy, i.e. how scattered the directional distribution is, with $\alpha = 1.0$ meaning all vectors share the same direction and $\alpha = 0$ representing a uniform distribution across all directions. We term α the ‘‘anisotropy intensity factor’’ in the current paper. These two variables are analogous to the concepts of ‘‘mean’’ and ‘‘coefficient of variation’’, respectively, in statistics. Furthermore the α can be shown to be proportional to the norm of the deviatoric part of the fabric tensor, an entity of great importance in the theory developed by Li and Dafalias (2012). The chief difference between the aforementioned approaches of mapping fabric tensors to PDF’s is essentially the different assumed analytical formats of the PDF’s. The accuracy of each mapping is dependent on the actual physical distribution of the microstructural features.

It is interesting to note that although the concept of fabric tensor was developed in the early 1980’s, the use of these two variables in the characterization of 2D orientation data has a substantially longer history. In Curray’s seminal work (1956), the following two variables were defined:

$$\bar{\theta} = \frac{1}{2} \arctan \frac{\sum \sin 2\theta}{\sum \cos 2\theta} \quad (7)$$

$$L = \frac{1}{C} \sqrt{(\sum \sin 2\theta)^2 + (\sum \cos 2\theta)^2} \quad (8)$$

where $\bar{\theta}$ is the quantity defined earlier as the major principal direction, and L , termed the ‘‘vector length’’, can be shown to have the same value as $\alpha = F_I - F_{II}$ by simple trigonometric relations. Therefore,

the concept of fabric tensor can be seen as a reincarnation of Curray's method from a statistical perspective. However, the generalization of fabric tensors from 2D to 3D is very straightforward whereas that of Curray's quantifications is not.

2.3 The choice of microstructural entities for constructing fabric tensors

At least three classes of microstructural quantities, including particle long axis orientations, inter-particle contact normal directions, and void shapes, have been used to construct fabric tensors. Each class of these quantities has some apparent advantages. It is widely recognized that the preferred alignment of **particle long axes** with the bedding plane is the primary source of inherent fabric anisotropy (Oda, 1972a, 1972b; Yang et al., 2008). The mechanism supporting the use of **contact normals** is that when the direction of the contact force deviates from the contact normal direction as a consequence of stress state evolution, the stability of this contact decreases with increasing likelihood of sliding or rolling. The role of **void shapes** in determining granular material mechanical behavior is less apparent. Since voids are simply the space that is not filled by the solid phase, the evolution of void spaces can be seen as a result of the evolution of the solid phase. Therefore, the relationship between the void space characteristics and material mechanical behavior is somewhat indirect. However, an indirect relation could still result in a strong and definitive correlation, making void-based fabric tensor potentially useful, especially when it is convenient to measure. Moreover, if hydrological properties of a material are concerned, such as anisotropic permeability, the role of fabric anisotropy in terms of void shapes becomes direct (Berkowitz and Ewing, 1998). Note that the void ratio in all cases can be considered as a separate scalar-valued fabric measure not related to orientational characteristics, but of fundamental importance for the mechanical response. In the case of void-based fabric tensors though, void ratio can be associated with the isotropic part of such tensors if an appropriate weight is used (Li and Li, 2009).

An interesting question to ask is whether one class of fabric tensors is intrinsically superior to another one. The ultimate criterion for evaluating the merits of a fabric tensor is, of course, *its ability to capture the most essential microstructural features that dictates material behavior with a small number of parameters*. However, if we put the development and application of fabric tensors in the context of the evolution of experimental and numerical research methods for geomechanics, we see that the choice of fabric tensors by a given study is usually driven by practicality rather than physical or mathematical merits.

One of the first studies concerning fabric anisotropy in sand was published by Oda in a series of papers (Oda 1972a, 1972b). In these studies, fabric anisotropy was quantified in terms of particle orientations observed on thin sections. Both the use of thin sections and the characterization of particle orientations seemed to have followed established conventions in the study of sedimentary rocks by geologists (Curray, 1956; Gipson, 1965). In fact, the term "fabric" was likely inherited from geology nomenclature (Friedman, 1965; Laird, 1970). Whereas it is possible to infer 3D particle orientation characteristics from 2D thin section images following stereological principles, information regarding inter-particle contacts in 3D is mostly lost in 2D thin sections. Therefore, this tradition could not have lead to the study and quantification of contact normals. The use of contact normal directions was associated with the emergence of DEM simulation of granular materials. Most DEM models (e.g. Cundall and Strack, 1979) use circular or spherical particles, for which particle orientations cannot be defined. On the other hand,

contact normal direction information can be easily extracted from DEM simulation results, and thus became a popular choice.

Void-based fabric measurements were mainly developed in the study of bone tissues (Harrigan and Mann, 1984). In porous media such as bones and porous rocks, the solid phase is continuous, and quantities such as particle orientations or inter-particle contacts are inapplicable. Voids in these porous media have a “discrete” appearance, especially in 2D sections, and are therefore more suitable for fabric characterization than the solid phase is. Although microstructure of granular materials is remarkably different from that of bone tissues, the techniques developed for characterizing void space geometry anisotropy of the latter can be easily applied to the former. Void-based fabric characterization also enjoys certain advantages in the analysis of CT (computed tomography) images. Probing void shapes in 3D CT data using line intercept-based algorithms (e.g. Muhunthan and Chameau, 1997; Inglis and Pietruszczak, 2003; Ghedia and O’Sullivan, 2012) is considerably easier than quantifying particle orientations. The latter requires individual particles to be reconstructed using image segmentation techniques (e.g. Hall et al., 2010). Measuring contact normal direction in CT images is even more difficult because it requires very high local accuracy in particle surface reconstruction in order to resolve the curvatures and corresponding tangent planes.

Definitive relations or correlations between these three classes of fabric tensors could be very useful. Such relation or correlation, if it exists, will enable scientists to quantify the microstructural features that are easy to measure and derive fabric tensors that are directly useful for constitutive modeling. A recent study (Fu and Dafalias, 2011b) on the fabric evolution in granular materials consisting of elongated particles observed very strong and consistent correlations between particle orientation- and contact normal-based fabric tensors along all the evolution paths evaluated. The major principal directions of these two tensors are approximately orthogonal to each other. a_p and a_n , representing anisotropy intensity of particle orientations and contact normal directions, respectively, are also highly correlated. Such correlations apparently do not apply to non-elongated particles, and void-based fabric tensors were not considered in that paper. Li et al. (2009) suggested strong correlation between anisotropy in contact normal and that in void shape, and suggested such correlation is affected by particle orientation distribution. That study did not attempt to systematically quantify this correlation though. In the current study, we investigate potential correlations among all three classes of fabric tensors, particularly those between the contact normal-based fabric tensor and a void-based fabric tensor for non-elongated particles.

3. Modifications to a void-based fabric tensor

The void-based fabric tensor used in the present study is largely based on a definition proposed by Li and Li (2009), which has been applied in those authors’ subsequent work (Li et al., 2009). However, some minor modifications as described below are made to enrich the original definition.

The backbone of Li and Li’s fabric tensor definition is a special tessellation of the domain occupied by the granular material. This tessellation is also the key feature that differentiates this fabric tensor definition from other graph-based void fabric tensors (e.g. Konishi and Naruse, 1988; Kuhn, 1999). The tessellation uses inter-particle contact points as nodes. Pseudo-contact points are inserted when necessary to ensure that no edge of the Delaunay triangles intersects edges of the polygon constructed by the contact points of any particle. The pseudo-contact points must be along the edges of these polygons. The **resulting**

tessellation system is called the “geometrical tessellation” by Li and Li. The next step is to group the triangles belonging to the same solid particle into “solid elements” and group the rest of the triangles into individual “void elements” to result in the so called “physical tessellation”. This process is illustrated in Figure 1. Li and Li also constructed a “solid cell” system and a “void cell” system based on the physical tessellation. Their definition of the fabric tensor is based on features of the void cell system. However, we found that the void elements in the physical tessellation contain sufficient information for quantifying the voids space characteristics, and thus the current study does not make reference to the void cell system.

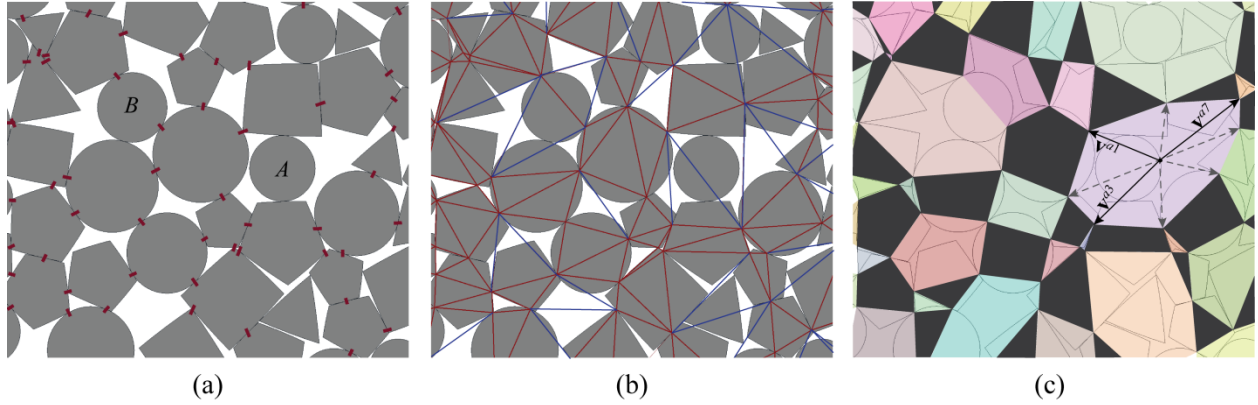


Figure 1 Construction of the physical tessellation of a 2D particle assembly. This illustration is based on a mix of circular disks, triangles, quadrilaterals, and pentagons used in section 5.1. (a) The particles (gray) and the void space (white) between them. The short thick lines denote the locations of inter-particle contacts and the contact force directions. (b) The Delaunay tessellation of the domain based on contact points. The two ends of the dark red lines belong to the same particle and the two ends of the blue lines belong to different particles. (c) The constructed physical tessellation of the granular assembly. The void elements are shown in random colors while the solid elements are in black. Eight void vectors for void element a are shown and three of them are denoted as \mathbf{v}^{a1} , \mathbf{v}^{a3} , and \mathbf{v}^{a7} , respectively

The void elements resulting from the above procedure not only contain the physical void space in the material, but also contain certain parts of the solid particles. If a particle does not contact any other particles or it has only one contact point, this particle is enclosed in a void element. If a particle has only two contact points, then no solid element can be constructed for it; it is split along the line connecting the two contact points by the tessellation, and the two pieces are included in two adjacent void elements. Particle A and particle B in Figure 1(a) are examples of these two scenarios, respectively. Note that particle A is very close to two neighbor particles as seen in the figure but no real contacts exist between them.

The objective of the fabric tensor formulation based on this physical tessellation system is to statistically quantify the shapes and orientations of the void elements. It is possible to treat each void element as a microstructural “entity” and directly calculate its shape and long axis orientation. The formulation for the corresponding fabric tensor would be essentially the same as that based on particle orientations. An alternative method as presented in Li and Li formulates a fabric tensor based on “void vectors”. A void vector, as originally defined by Li and Li, is the vector from the center of a “void cell” to a contact point around this void cell. In the current study, we use the center of the “void element” instead as the origin of the void cell, because as already mentioned the void elements contain all the information needed for the characterization of the void structures. The fabric tensor definition by Li and Li is

$$\mathbf{F}_v = E_0 \oint_{\Omega} \bar{v}(\mathbf{n}) \mathbf{n} \otimes \mathbf{n} d\Omega \quad (9)$$

where \mathbf{n} is the unit vector representing the direction of a void vector; E_0 is a normalization factor to scale the trace of the tensor; and $\bar{v}(\mathbf{n})$ is the mean length of void vectors along a given direction. Comparing equation (9) with equation (1), we find that the $\mathbf{n} \otimes \mathbf{n}$ term is weighted by the mean vector length, instead of the probability density as in equation (1). The benefit of using the vector length as the weight is rather evident, as the orientations of the void vectors are not sufficient for determining the shapes of the void elements. To consider a highly idealized yet illustrative case, even if the void elements are all circular in shape (i.e. isotropic), equation (1) can still yield a highly anisotropic quantification if the void vectors are not uniformly distributed. However, ignoring the probability density of void vector directions in equation (9) results in some other undesirable consequences. For instance, if along a certain range of directions the probability density of void vectors is very small (i.e. void vectors are rare along this angle range, possibly just one), but the few void vectors in this range are very long, this small number of void vectors will have an unreasonably high impact on the fabric tensor value because their small number will not be reflected in the calculation part of equation (9) along \mathbf{n} . This consequence of the continuum formulation is evident in the corresponding discrete form of the fabric tensor in Li and Li (2009) that reads

$$\mathbf{F}_v = \frac{E_0}{N_v} \sum_{a=1}^{N_v} \frac{v^a \mathbf{n}^a \otimes \mathbf{n}^a}{E_v(\mathbf{n}^a)} \quad (10)$$

where N_v is the total count of void vectors in a particle assembly; a is the index of individual void vectors; v^a is the length of the a^{th} void vector. Since the probability density function $E_v(\mathbf{n}^a)$ is in the denominator, it implies that a void vector along a more “popular” direction would have a smaller effect on the fabric tensor value. This is somewhat unreasonable since all void vectors should be “created equal”. Moreover, the calculation of the fabric tensor according to equation (10) requires *a priori* knowledge of the probability density function, whereas an important role of fabric tensors is to provide a concise way of expressing the probability distribution. Finally if one imagines that the particles scale up or down in size with no other change of the aggregate, so will the voids and the void vector lengths, and consequently it follows from Eqs. (9) or (10) that the norm of the fabric tensor will change by the scaling factor while one expects that such an aggregate must have a fabric tensor that is invariant in regards to this kind of scaling.

We argue that it is more reasonable to consider both the directional probability distribution and the average length of void vectors in constructing the fabric tensor. Using equation (4) as the template, we proposed a slightly modified version of the void-based fabric tensor. After being normalized to a unity-trace form, we have

$$\mathbf{F}_v = \frac{\iint_{\Omega} E(\mathbf{n}, v) \mathbf{v} \mathbf{n} \otimes \mathbf{n} d\Omega dv}{\iint_{\Omega} E(\mathbf{n}, v) v d\Omega dv} \quad (11)$$

where \mathbf{v} is a void vector; v is the length of the void vector; and \mathbf{n} is the unit vector representing the direction of the void vector. Its discrete summation form Eq.(11) reads:

$$\mathbf{F}_v = \frac{\sum_{a=1}^{N_v} v^a \mathbf{n}^a \otimes \mathbf{n}^a}{\sum_{a=1}^{N_v} v^a} \quad (12)$$

where N_v is the total number of void vectors. Notice that equations (11) and (12) are invariant with respect to a scale change of particles and voids. \mathbf{F}_v in subsequent section of the current paper is based on this modified definition.

4 Correlation between contact normal- and void-based fabric tensors for circular particles

Based on the description in section 3, we see that the definition of this void-based fabric tensor only uses information regarding the locations of inter-particle contact points, but not information on the normal directions. No apparent relation between \mathbf{F}_n and \mathbf{F}_v can be directly established through their definitions. In the current section, we first identify a possible correlation between \mathbf{F}_n and \mathbf{F}_v through the simulation of biaxial compression tests of circular particles assemblies. We then test this correlation by varying a number of parameters of the granular assembly and test conditions.

4.1 Initial exploration of the \mathbf{F}_n - \mathbf{F}_v correlation

In the first suite of numerical examples, we simulate granular assemblies consisting of circular particles starting from different initial densities. Each assembly contains approximately 20,000 disks with diameters (D_p) randomly distributed between 0.3 mm and 1.0 mm. This particle size distribution is denoted as *distribution I*, and some other distributions will be introduced in section 4.3. The inter-particle friction angle ϕ_p is 35°. We first simulate the pluviation process routinely performed in soil laboratories for fabricating sand specimens. Relatively high numerical damping is used to obtain a loose specimen. Then the sample is consolidated using various methods towards different initial densities ($e_0 = 0.247, 0.230, 0.212, 0.203, 0.193, \text{ and } 0.184$) under an isotropic confining stress of 100 kPa. These six specimens are denoted as specimens A1 through A6. The consolidated samples have a height-to-width ratio of 2.5. The confining pressure is applied through zero-friction rigid walls that numerically simulate servo-controlled loading systems in real-world laboratories. After consolidation is finished, compression loading is applied by the upper and lower walls, and the two side walls are controlled in a way to maintain a constant mean stress of 100 kPa. Other aspects of the numerical models are similar to results published in our previous studies (Fu and Dafalias, 2011a; Fu et al., 2012) and are not repeated here.

The deformation patterns of three of the six simulated specimens are shown in Figure 2. Selected particles are “dyed” black to form a regular grid pattern in the undeformed specimens. The general deformation patterns including deformation localization (shear-banding) can be clearly visualized through the deformed patterns of the grids. The initially dense specimens tend to form distinct shear bands, which is consistent with common soil mechanics knowledge. The specific shear-banding pattern observed is a result of the kinematic constraints imposed by the rigid walls.

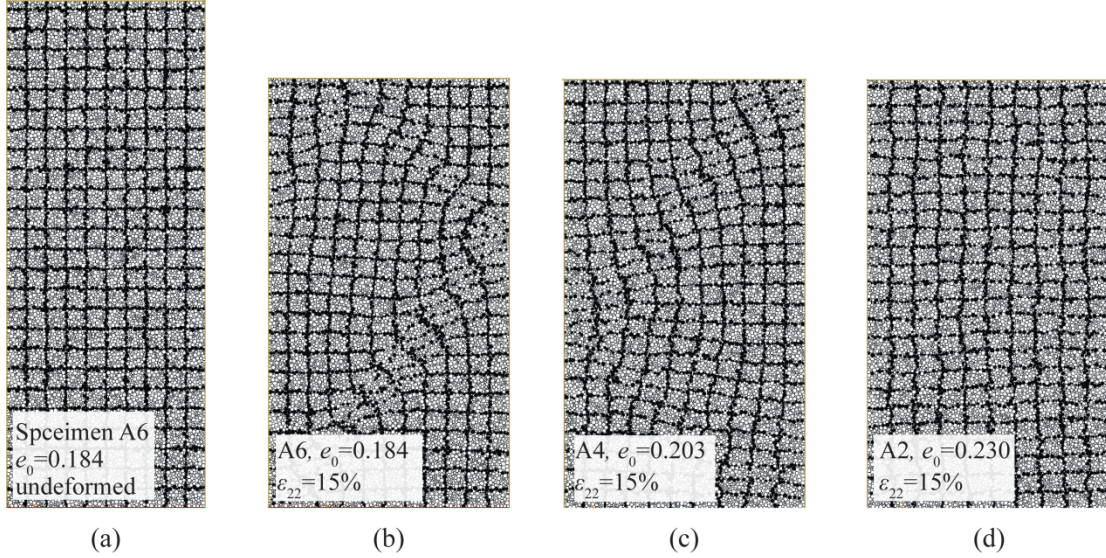


Figure 2 Deformation patterns of selected specimens in the first suite of simulations.

The evolutions of the principal stress ratio and average void ratio of the six specimens are shown in Figure 3(a) and (b). The mechanical behavior simulated is qualitatively representative of typical sands: The stress ratio of dense sand first reaches a peak value at a relatively small axial strain (ϵ_{22}), and then decreases to a steady state value. The stress ratio of loose sand monotonically and gradually increases to the same steady state value. The steady state stress ratio is approximately 1.8 for the material simulated. In terms of the evolution of average void ratio, dense sand dilates and loose sand contracts. The mean void ratio in the steady state seems to be dependent on the initial void ratio. As revealed by our previous study (Fu and Dafalias, 2011b), this is a result of shear-banding, because the critical state is reached by the material in shear bands but not the remaining parts of the specimen. This argument is further supported by the deformation patterns shown in Figure 2: Initially denser specimens show distinct shear-bands; loose specimens show complicated and diffuse shear band patterns but the deformation pattern is not uniform either. Nevertheless the loose samples, having less inhomogeneity than dense, converge towards a common critical void ration of about 0.23. Although the focus of the current paper is not to discuss such mechanical behaviors, by showing that the simulation results are consistent with common soil mechanics knowledge we reassure the effectiveness of using particle-based simulations to study real granular material behaviors.

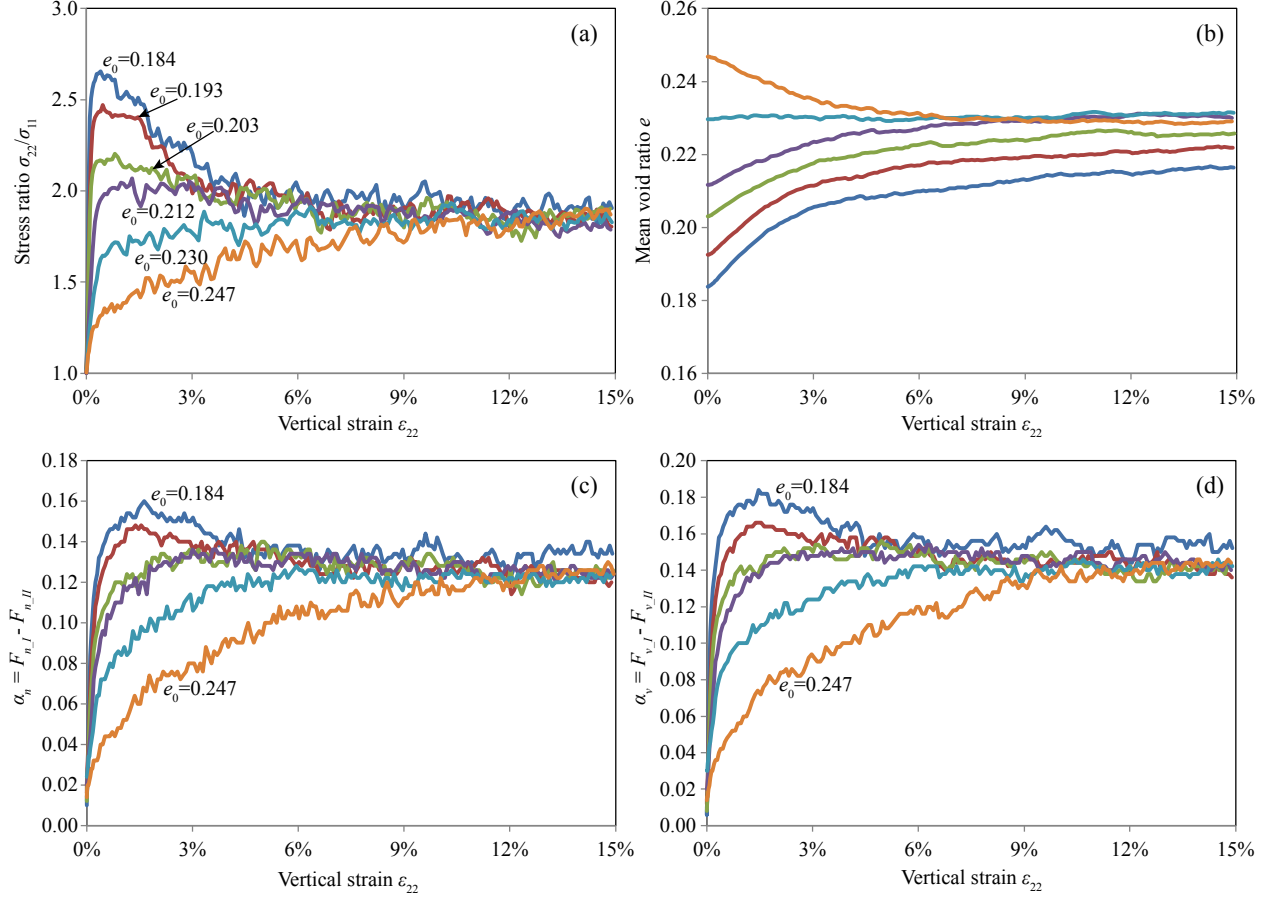


Figure 3 The evolutions of (a) principal stress ratio σ_{22}/σ_{11} , (b) average void ratio e , (c) contact normal-based fabric anisotropy intensity factor α_n , and (d) void-based fabric anisotropy intensity factor α_v with respect to axial strain for specimens with different initial densities (specimens A1 through A6).

As described in section 2.2, a 2D unity-trace fabric tensor only has two degrees of freedom. The loading boundary condition dictates that the mean principal direction must be vertical, so the anisotropy intensity factor (α_v or α_n) alone can determine the full fabric tensor. The evolutions of α_n and α_v are shown in Figure 3(c) and (d), respectively. The similarity between the α_n curve and the α_v curve for each specimen is quite striking. The α_n - α_v correlation for all six specimens is plotted in Figure 4(a), where a simple and strong linear correlation, $\alpha_v = 1.144\alpha_n$, emerges with a very high R^2 (coefficient of determination) value of 0.99. Note that in all the linear regression analyses in the current paper, we force the regression line to go through the coordinate origin, which represents the isotropic fabric. The correlation is independent of the initial void ratio, the subsequent void ratio change, and stress state evolution in each specimen. It is well-known in soil mechanics that dense sand under high mean stress behaves similarly to loose sand under low mean stress, so we can infer that the same α_n - α_v correlation holds for different mean stress levels, although all the six simulations are performed at the same mean stress level.

Note that the principal directions of fabric tensors inside oblique shear bands deviate from the vertical and horizontal directions. Section 4.5 reveals that the proposed correlation also holds for normal components in addition to principal components of the fabric tensors. Therefore, this deviation in the shear bands has no effects on the regression results above.

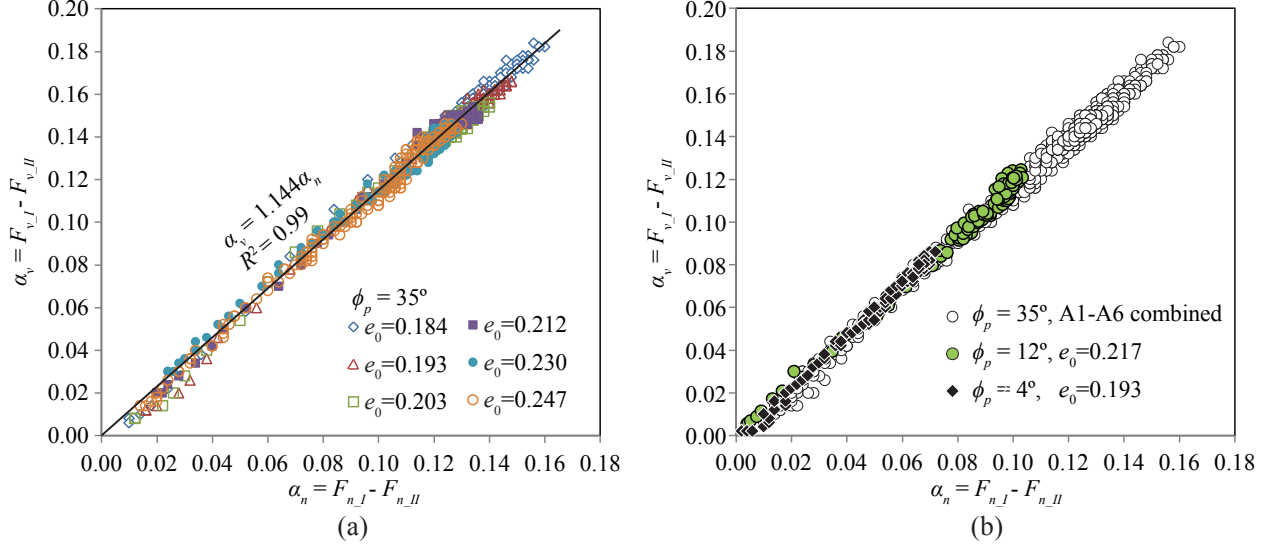


Figure 4 The α_n - α_v correlation for (a) the six specimens with different initial void ratios but the same inter-particle friction angle ϕ_p of 35° and (b) specimens with different ϕ_p values.

4.2 The effects of inter-particle friction angle

In this section we investigate whether the inter-particle friction angle ϕ_p affects the α_n - α_v correlation. As an internal variable, ϕ_p for real granular materials is determined by the mineralogy and surface texture of particles (Mitchell and Soga, 2005). In DEM models, it is a parameter determining the frictional strength of particle-particle contacts. $\phi_p=35^\circ$ is used for the six simulations in section 4.1. In the current section, we test specimens consisting of the same particles but with $\phi_p=12^\circ$ and 4° . These values are probably too low for real geomaterials, but we use these extreme values to cover the parameter space. Since we have shown that the α_n - α_v correlation does not vary with densities, we only simulate one initial density at each ϕ_p level. The two specimens, with $\phi_p=12^\circ$ and 4° , have initial void ratios of 0.217 and 0.193, respectively under an isotropic stress of 100 kPa, and we denote them as specimens B1 and B2, respectively. The loading scenario is similar to that in the previous section. The steady (or critical) state void ratios are 0.202 and 0.184 respectively, and the steady state principal stress ratios are 1.75 and 1.5, respectively. The α_n - α_v correlation for these two simulations is shown in Figure 4(b) on top of the data for specimens A1 through A6. Although the highest intensity of fabric anisotropy that a specimen achieves generally decreases as ϕ_p decreases, it is evident that exactly the same correlation holds for different inter-particle friction angles. Since the eight specimens exhibit a wide variety of mechanical behaviors but share the same particle geometry (i.e. shape and size distribution), the fact that exactly the same α_n - α_v correlation holds for all of them suggests that the root of this strong correlation is inherently “geometrical”, rather than mechanical.

4.3 The effects of particle size distribution

The simulations in sections 4.1 and 4.2 use the same particle size distribution (distribution I), with disk diameters randomly distributed between 0.3 mm and 1.0 mm. We now investigate the α_n - α_v correlation for three more distributions (distributions II to IV). All four distributions have the same maximum particle

diameter of 1.0 mm. The smallest particle diameter is 0.5 mm for distribution II, and 0.8 mm for distribution III. All particles for distribution IV have the same diameter of 1.0 mm. The four particle size distributions are illustrated in Figure 5. For each of distributions II to IV, only one constant-mean stress biaxial compression test is performed. The three simulations are denoted as C1, C2, and C3. No particular attention is paid to the initial void ratios or the mechanical behavior, since we have observed that these factors do not affect the α_n - α_v correlation. The linear regression analysis results are summarized in Table 1. The results indicate that similar α_n - α_v correlations hold for all the particle size distributions tested. The regression coefficient, namely the ratio between α_v and α_n , is slightly affected by the particle size distributions. As the range of particle sizes becomes narrower, the ratio appears to approach unity.

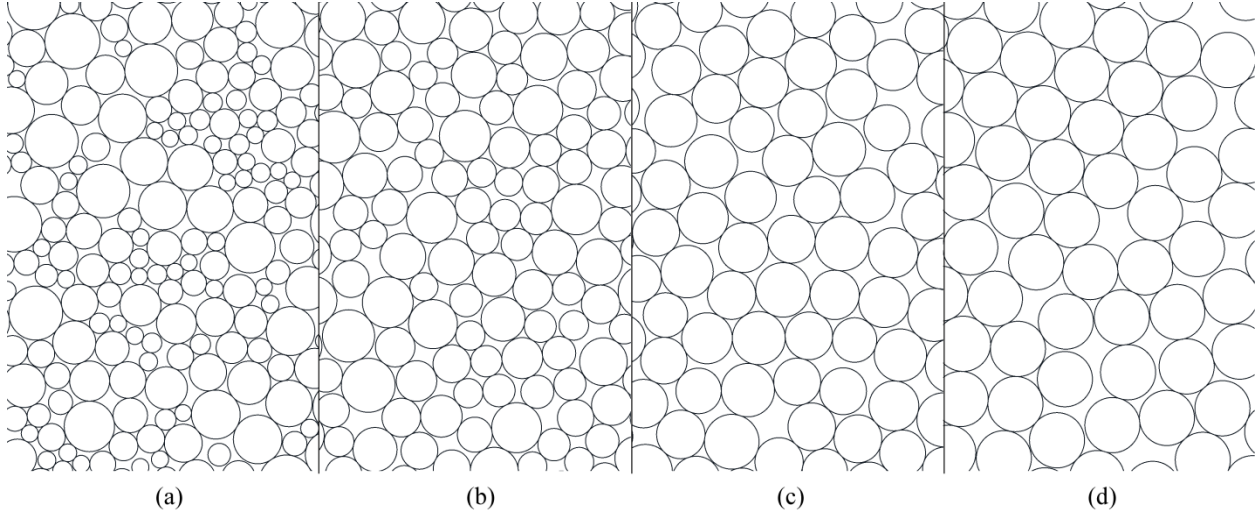


Figure 5 Different particle size distributions investigated in this study. (a) Distribution I with particle diameters ranging between 0.3 mm and 1.0 mm; (b) Distribution II, between 0.5 mm and 1.0 mm, (c) Distribution III, between 0.8 mm and 1.0 mm, and (d) Distribution IV, 1.0 mm monodisperse.

Table 1 α_n - α_v correlation for particle assemblies with different particle size distributions

Distribution	Specimens	Min. D_p	Max. D_p	α_n - α_v correlation	R^2 value
I	A1-A6, B1, B2	0.3 mm	1.0 mm	$\alpha_v = 1.146 \alpha_n$	0.994
II	C1	0.5 mm	1.0 mm	$\alpha_v = 1.060 \alpha_n$	0.986
III	C2	0.8 mm	1.0 mm	$\alpha_v = 1.012 \alpha_n$	0.983
IV	C3	1.0 mm	1.0 mm	$\alpha_v = 1.019 \alpha_n$	0.968

4.4 Test correlation for rotating fabric tensors

In the aforementioned analyses, the principal direction of the fabric tensor is along the loading direction, so the variation of the fabric tensor is fully represented by the evolution of the α value alone. In this section, we load a specimen with a continuously rotating stress boundary condition, expecting that the fabric tensors rotate along with it. We investigate the relationship between the contact normal- and void-based fabric tensors under this condition.

In real world laboratories, the rotating stress boundary is applied using hollow cylinder apparatus (Hight et al., 1983; Tong et al., 2010). In DEM simulation, arbitrary stress boundary conditions can be directly applied to a particle assembly if the particles along the assembly boundary are identified. In this study, we create a particle assembly using the same parameters as those in specimens A1 to A6 (section 4.1) and denote it as specimen D. The assembly is composed of 18,500 particles and is circular in shape itself as show in Figure 6. The algorithms for identifying boundary particles and directly applying stress boundary conditions to those particles have been successfully used in our previous studies (Fu and Dafalias, 2011a; Fu et al., 2012) when applying stress-controlled boundary conditions in biaxial compression simulations. The two principal components of the stress applied are $\sigma_I = 130$ kPa and $\sigma_{II} = 70$ kPa, with compression being positive. In the beginning of the simulation, σ_I is in the vertical direction, and then the principal axes of the applied stress slowly rotate counterclockwise. Figure 6 shows the force chains in the particle assembly in two states. In the initial state, the fabric tensors and the stress tensor are coaxial due to the symmetry of the system. As the stress axes rotate, the two fabric tensors should evolve accordingly. To quantify this process, we calculate the orientation angles (angles measured positive counterclockwise with respect to the horizontal direction) of the major principal directions of the stress tensor ($\bar{\theta}_s$), the contact normal-based fabric tensor ($\bar{\theta}_n$), and the void-based fabric tensor ($\bar{\theta}_v$) and plot those in Figure 7(a). Note that a small number of particles near the surface of the assembly tend to move excessively due to the lack of kinematic constrains, but this does not affect the overall stress and fabric of the particles inside the assembly. In the summations for calculating the stress tensor and fabric tensors, we only include the 11,000 particles at the center of the specimen to avoid the influence of these surface particles.

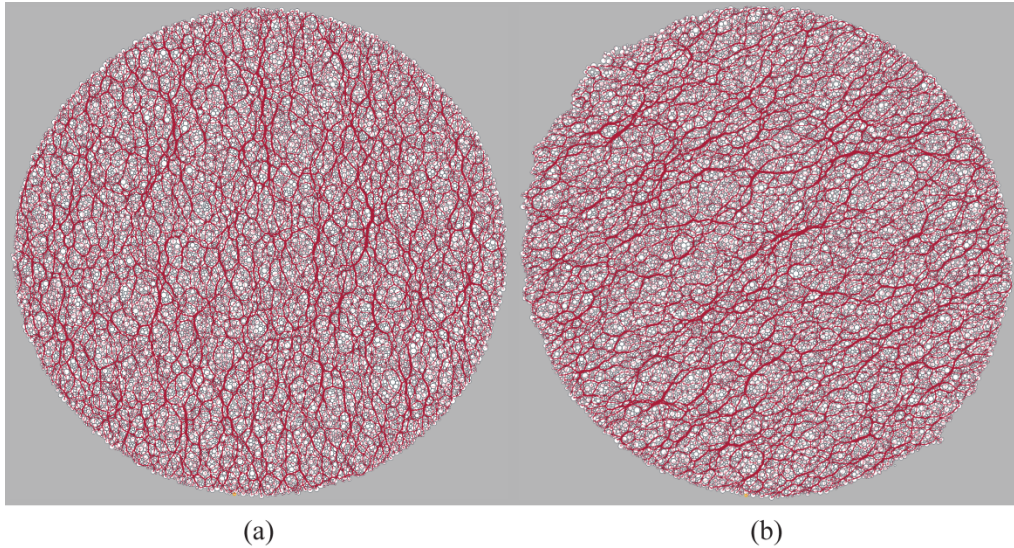


Figure 6 Force chains in the specimen subjected to rotating stress boundary condition, (a) in the initial state and (b) after the principal stress axis have rotated 120° counterclockwise.

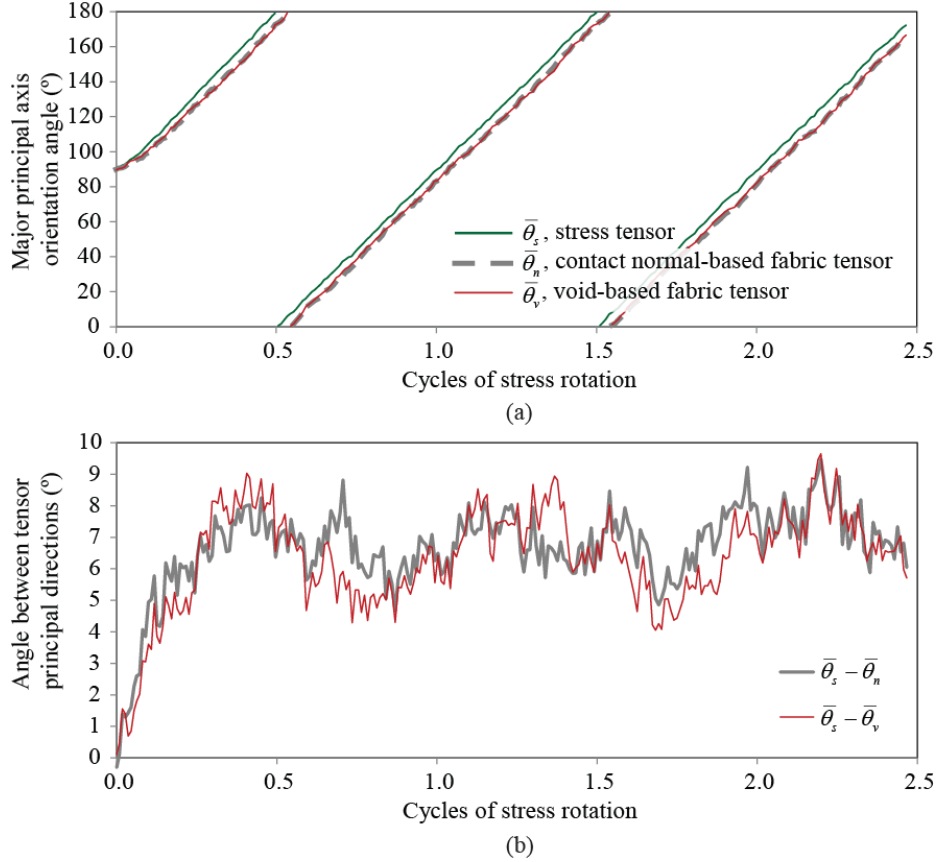


Figure 7 Evolution of the fabric tensors' principal direction as the stress tensor rotates. (a) The orientation angle of the stress tensor and fabric tensors; and (b) the lag of orientation angles between the two fabric tensors and the stress tensor.

In Figure 7(a), we see that the principal axes of the two fabric tensors rotate along with the stress tensor at approximately the same rate, as expected. However, there is a lag of a few degrees between the principal axes of the fabric tensors and that of the stress tensor, whereas the two fabric tensors seem to be coaxial. For more accurate analysis, we plot the lags of $\bar{\theta}_s - \bar{\theta}_n$ and $\bar{\theta}_s - \bar{\theta}_v$ in Figure 7(b). We see that the lags increase from zero as the stress rotation starts and stabilize after approximately a half cycle of rotation (a cycle is 180° due to rotational symmetry). After stabilization, the lags show both long-period and high-frequency fluctuations. The period of the low-frequency fluctuation is one cycle of rotation. The lag between $\bar{\theta}_s$ and $\bar{\theta}_n$ and that between $\bar{\theta}_s$ and $\bar{\theta}_v$ are almost identical in terms of long-period fluctuation, although the high-frequency components do not exactly match. Since the high-frequency fluctuation should be associated with transient processes such as momentarily unbalanced forces associated with force chain buckling and numerical noises, we conclude that the two fabric tensors are indeed coaxial. During the stress rotation, the intensity of fabric anisotropy represented by the α value also have some minor fluctuation as shown in Figure 8(a), and the linear regression result $\alpha_v = 1.143\alpha_n$ is almost identical to the correlations obtained in sections 4.1 and 4.2 for the same virtual material. Because the magnitude of the α value's variation is relatively small and comparable to the noise level during stress rotation with fixed stress ratio, the R^2 value is not very high. However, the correlation is rather evident and consistent with that based on biaxial compression simulation results.

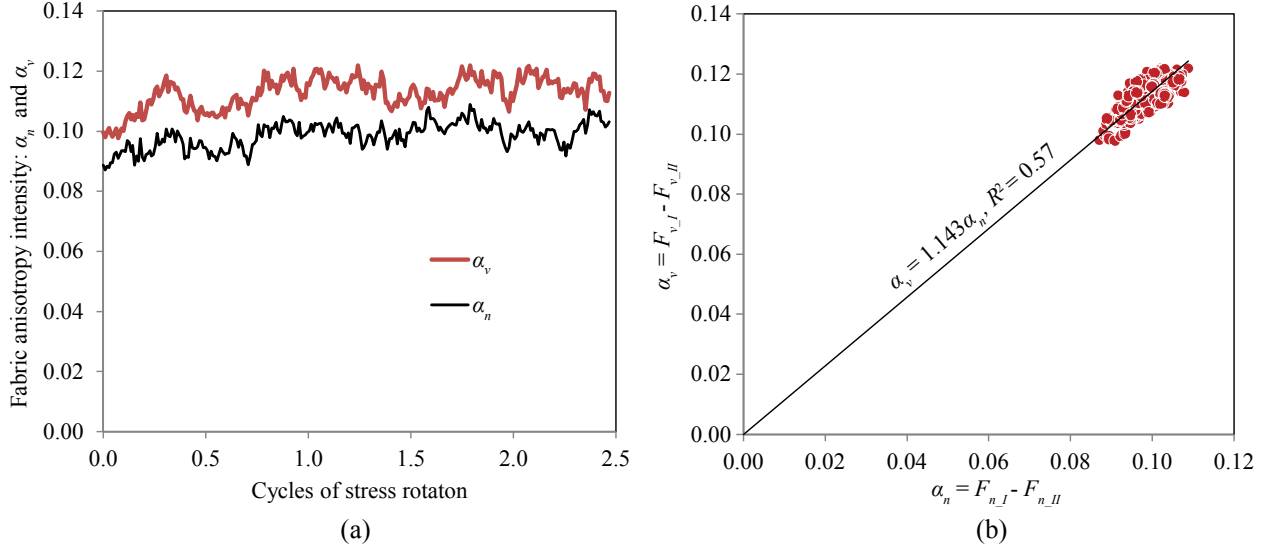


Figure 8 Intensity of fabric anisotropy during stress rotation. (a) The evolution of α_n and α_v with respect to rotation cycles; and (b) the correlation between α_n and α_v .

4.5 Generic relationships for arbitrary components of fabric tensors

So far we have demonstrated that the \mathbf{F}_v tensor and \mathbf{F}_n tensor are coaxial and there is a simple and strong linear correlation between their principal components under all conditions tested. If we assume that the correlation has the form of $\alpha_v = \lambda \alpha_n$, we can derive the generic relationship between the \mathbf{F}_v tensor and \mathbf{F}_n tensor in an arbitrary coordinate system as follows. First, we establish the reference coordinate system $x - y$ coaxial with the fabric tensors, and the fabric tensor \mathbf{F} (can be either \mathbf{F}_v or \mathbf{F}_n) in this coordinate system reads

$$\mathbf{F} = \begin{bmatrix} F_I & 0 \\ 0 & F_{II} \end{bmatrix} \quad (13)$$

In an arbitrary coordinate system $\bar{x} - \bar{y}$ rotating counterclockwise by angle θ from the reference coordinate system, the fabric tensor becomes $\bar{\mathbf{F}} = \mathbf{R}^T \mathbf{F} \mathbf{R}$, where \mathbf{R} is the rotation matrix as

$$\mathbf{R} = \begin{bmatrix} \cos \theta & -\sin \theta \\ \sin \theta & \cos \theta \end{bmatrix} \quad (14)$$

Noticing $F_I = (1 + \alpha)/2$ and $F_{II} = (1 - \alpha)/2$, we have

$$\begin{aligned} \bar{\mathbf{F}} &= \begin{bmatrix} F_I \cos^2 \theta + F_{II} \sin^2 \theta & (F_I - F_{II}) \cos \theta \sin \theta \\ (F_I - F_{II}) \cos \theta \sin \theta & F_I \sin^2 \theta + F_{II} \cos^2 \theta \end{bmatrix} \\ &= \begin{bmatrix} 0.5(\cos^2 \theta - \sin^2 \theta)\alpha + 0.5 & \alpha \cos \theta \sin \theta \\ \alpha \cos \theta \sin \theta & 0.5(\sin^2 \theta - \cos^2 \theta)\alpha + 0.5 \end{bmatrix} \end{aligned} \quad (15)$$

Because both $\bar{\mathbf{F}}_v$ and $\bar{\mathbf{F}}_n$ follow the same format as equation (15), we can establish the following relationship between all the components of these two tensors in an arbitrary coordinate system

$$F_{v_{ij}} = \begin{cases} \lambda(F_{n_{ij}} - 0.5) + 0.5, & \text{if } i = j \\ \lambda F_{n_{ij}}, & \text{if } i \neq j \end{cases} \quad (16)$$

4.6 Directional distributions of contact normals and void vectors

As elaborated in section 2.2, a fabric tensor essentially quantifies statistical characteristics of the directional distribution of the microstructural entities that the fabric tensor is based on. The major principal axis of a fabric tensor is in fact the mean orientation of the microstructural entity whereas the anisotropic intensity (α value) is analogous to the coefficient of variation in statistics. Given the extremely strong correlation between \mathbf{F}_n and \mathbf{F}_v discovered in the preceding sections, a question that naturally arises is whether there is a simple and direct relation between the direction distribution of contact normals and that of the void vectors.

In Figure 9 we plot rose diagrams of contact normals and void vectors for two simulations. Rose diagrams are frequency histograms plotted in a polar coordinate system, commonly used to visualize directional distributions in a concise and intuitive fashion. Consistent with the fabric tensor definitions used in the current study, the rose diagrams for contact normals are “unweighted” while those for void vectors are weighted by void vector lengths. The results presented are based on biaxial compression simulations of circular particles introduced in previous sections: A5 in section 4.1 and C3 in section 4.3. The main difference between these two specimens is the particle size distribution. Specimen A5 is composed of particle diameters ranging between 0.3 mm and 1.0 mm, whereas specimen C3 consists of monodisperse particles. For each simulation, we choose four representative states: State 0 is the initial state under isotropic confining stress; state 1 is approximately at halfway of the initial ascending segment of the α curve; State 2 is at the peak of the α curve; and State 3 is at the steady state where both the stress state and fabric tensor fluctuate around their respective steady state values as the specimens undergo continued deformation. It is interesting that before reaching the steady state value (corresponding to critical state from the perspective of stress ratio and void ratio), the fabric tensor norm measured by α acquires a higher value.

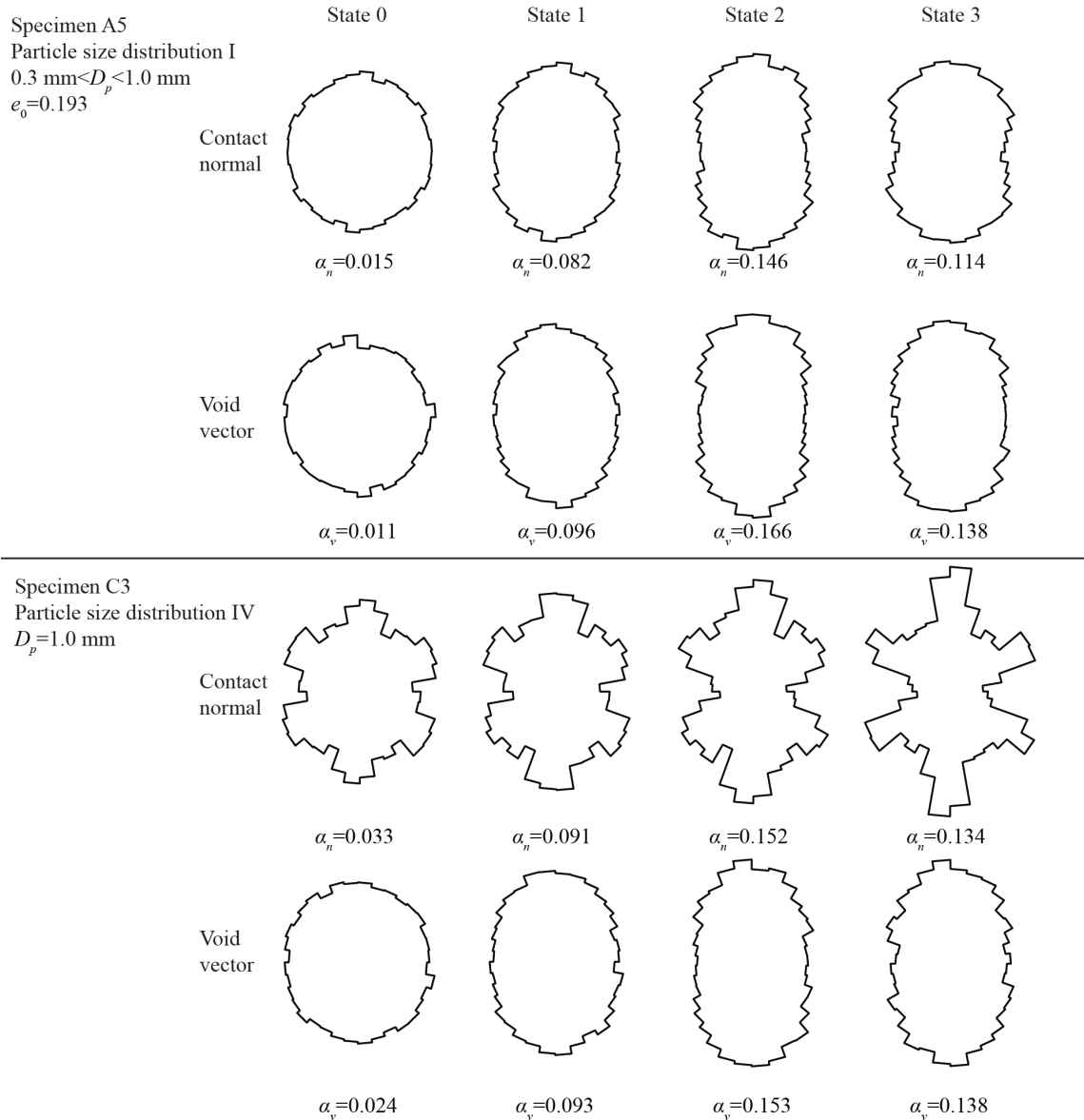


Figure 9 The evolution of directional distributions of contact normals and void vectors for two simulations, one with particle size distribution I (particle diameter D_p between 0.3 mm and 1.0 mm) and the other with distribution IV (monodisperse particles).

At State 0, all the rose diagrams are approximately circular in shape, representing largely isotropic fabric. As the intensity of fabric anisotropy increases, the rose diagrams elongates along the major principal direction. These two phenomena are shared by both simulations and both fabric tensors, as expected according to the definition of fabric tensors. The overall shape of contact normal-based rose diagram and that of the void vector-based rose diagram are very similar for specimen A5 at each selected state. The void vector-based rose diagrams are slightly more elongated than the contact normal-based rose diagrams, consistent with the regression result $\alpha_v = 1.146 \alpha_n$.

However, the contact normal-based rose diagrams for specimen C3 exhibit some striking yet interesting features. For this stimulation, contact normals appear to concentrate in three preferred directions,

approximately 30°, 90°, and 150° from the horizontal. The reason for this concentration is that during deposition and loading of the specimen, particles tend to form clusters in the so-called “hexagonal packing”, such as that visible at the upper left corner of Figure 5(d). Because hexagonal packing is the densest packing that monodisperse particles can achieve, once formed, these clusters are very stable and behave like rigid bodies. As the specimen deforms under loading, more and more particles are included in these clusters, so such concentration intensifies as the specimen deforms. This sort of concentration of contact normal directions also emerges from the results of specimen C2 (not shown), which has a relatively narrow range of particle sizes (0.8 mm to 1.0 mm), but the concentration is to a lesser extent than that of specimen C3. The void vector-based rose diagrams for this specimen, on the other hand, show no sign of such concentration. In fact, the void vector-based rose diagrams for the specimen C3 are very similar to those for A1 when the α_v values are similar.

These results indicate that there is not a simple relationship or mapping between the directional distribution of contact normals and that of void vectors. However, the simple correlations between the fabric tensors revealed in sections 4.1 to 4.4 hold despite the lack of such a direct relationship between the distributions. This is analogous to the fact in statistics that two populations can have the same mean and coefficient of variation but different distributions.

5 Relationships for non-circular particles

In this section we evaluate the correlation between different fabric tensors for non-circular particles.

5.1 Test the correlation on non-elongated particles

First, we evaluate the \mathbf{F}_n - \mathbf{F}_v relationship for non-circular particles that are not apparently elongated, namely those particles with an aspect ratio of nearly one. To this end, we create a particle assembly consisting of 1,200 disks, 1,200 triangles, 1,200 quadrilaterals, and 2,400 pentagons. The diameters of the bounding circles of these particles follow distribution I as described in section 4.1, namely ranging between 0.3 mm and 1.0 mm. The polygonal particles are first generated as regular polygons, and then some random perturbation is applied to the shapes to break the regularity. The perturbations are small enough that the particles are not significantly elongated. The particle shapes and size distribution can be visually assessed in Figure 10(a). Only one simulation of a biaxial compression test is performed, and the results show a clear linear correlation of $\alpha_v=1.165\alpha_n$ with a R^2 value of 0.99, as shown in Figure 10(b). Considering the largest particle size in this mix of particles is the same as that of distribution I while the smallest particle size is slightly smaller than that in distribution I, the slope of the α_n - α_v correlation (1.165) is very consistent with the trend identified in Table 1.

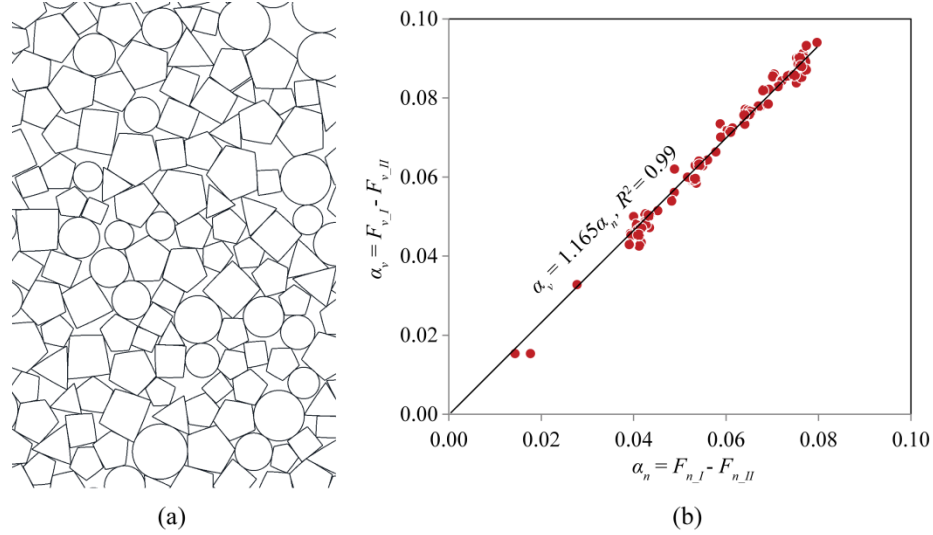


Figure 10 Results for a mix of disks, triangles, quadrilaterals, and pentagons. (a) Particle shapes and size distributions; and (b) the α_n - α_v correlation.

We conclude that the α_n - α_v correlation identified for the mix of particles with various shapes is essentially the same as that identified for circular particles in section 4, which eliminates the needs for further investigation of the effects of other variables that have been studied in section 4. The generalization of the correlation for noncircular particles is considered a remarkable advance, because a circle has a number of unique properties that differentiate it from all other 2D shapes. For instance, a branch vector (the vector pointing to a contact point from the particle center) and the contact normal share the same direction for circular particles, which is not valid for polygon particles. With the generalized results, we understand that the α_n - α_v correlation identified does not rely on those unique properties of circles.

5.2 Preliminary exploration for elongated particles

The relationships between fabric tensors for elongated particles are necessarily more complicated than that for non-elongated particles. We have to include the fabric tensor based on particle orientations in addition to the two tensors discussed in previous sections. The DEM simulation used here has been analyzed in two of our previous publications, as specimen “BC00” in Fu and Dafalias (2011b) and the only numerical example in (Fu and Dafalias, 2012). However, the previous analyses focused on granular material behaviors from perspectives different from that of the current paper.

In this simulation, the particle assembly is composed of 45,000 ellipse-shaped particles and all the particles have the same aspect ratio of 1:3. The long axis lengths are randomly distributed between 0.3 mm and 1.0 mm. The assembly is fabricated by simulating the air pluviation process (dropping the particles into a box from a fixed height under gravity force), as illustrated in Figure A3 of Fu and Dafalias (2011a). This process results in a strong tendency of the particles to align the long axes with the horizontal bedding plane. If more precise control of initial fabric is desired, some more recent methods can be utilized (Mollon and Zhao, 2012), but the pluviation simulation technique well suits the purpose of the current paper.

The virtual sample is first consolidated under an isotropic stress of 100 kPa. In this state, the fabric tensors based on particle orientations, contact normal directions, and void shapes are calculated as shown in Table 2. The four components of each fabric tensor in the given coordinate system as well as the major principal direction are shown. The high $\alpha=F_I-F_{II}$ values of all three tensors indicate strong fabric anisotropy of the material, which is an expected consequence of the highly elongated particle shape. The major principal direction of the particle orientation-based fabric tensor \mathbf{F}_p is largely horizontal, aligning with the bedding plane. The 0.6° error is due to inevitable imperfection in the sample fabrication process. The major principal axis of contact normal fabric tensor \mathbf{F}_n is vertical, perpendicular to the particle orientation-based tensor, a phenomenon extensively discussed in Fu and Dafalias (2011b). The major principal direction of the void-based tensor \mathbf{F}_v is horizontal in this case, which is the same as that of \mathbf{F}_p but perpendicular to that of \mathbf{F}_n . As shown in Figure 11, the void elements constructed based on Li and Li's (2009) method, which are randomly colored in Figure 11, tend to elongate along the bedding plane direction. This indicates that the strong \mathbf{F}_n - \mathbf{F}_v correlation expressed by equation (13) does not hold for elongated particles.

Table 2 Different fabric tensors for the elliptical particle assembly at the initial state

Method	F_{11}^0	F_{22}^0	F_{12}^0, F_{21}^0	$\bar{\theta}^0$	$F_I^0 - F_{II}^0$
Particle orientation	0.737	0.263	-0.0049	-0.6°	0.474
Contact normal	0.337	0.663	0.0013	89.8°	0.326
Void shape	0.629	0.371	-0.005	-1.2°	0.259

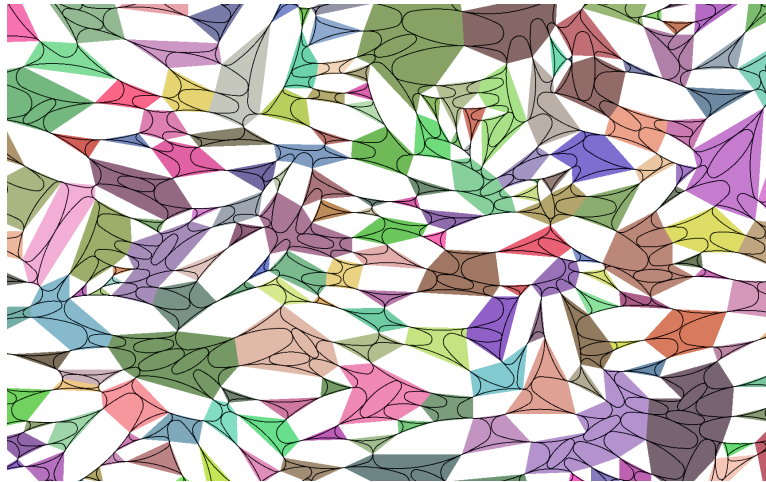


Figure 11 Void elements constructed for the elliptical particle assembly in the initial state with isotropic stress. Note that section 3 has provided a brief overview of the construction of the void elements.

We apply vertical compression to the specimen while maintaining the confining pressure (σ_{11}) at 100 kPa. The evolutions of the principal stress ratio (σ_{22}/σ_{11}) and the volumetric strain are shown in Figure 12. The deformation patterns of the specimen at four axial strain (ϵ_{22}) levels of 2.5%, 5%, 10%, and 15% are shown in Figure 13. At $\epsilon_{22}=2.5\%$, the stress ratio is at its peak and the deformation pattern is largely uniform. At $\epsilon_{22}=5\%$, the stress ratio is declining from the peak to its steady state value, and the dilation of

the specimen is close to an end. Meanwhile, the shear band development is clearly visible in this state. At the two larger strain levels, 10% and 15%, the specimen has reached its steady state, in which the deformation concentrates within the shear band with nearly constant stress state. The fabric evolution inside the shear band has been investigated in Fu and Dafalias (2011b) and the formation of the shear band as a process of multiple failure planes competing in this simulation have been studied in Fu and Dafalias (2012). We only focus on global fabric measurements in the current study.

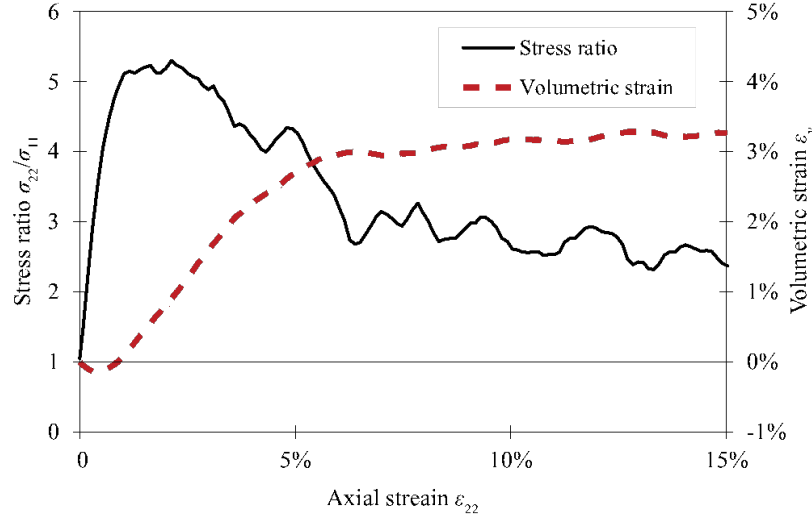


Figure 12 Mechanical behavior of the numerical specimen consisting of 45,000 elliptical particles deposited under gravity.

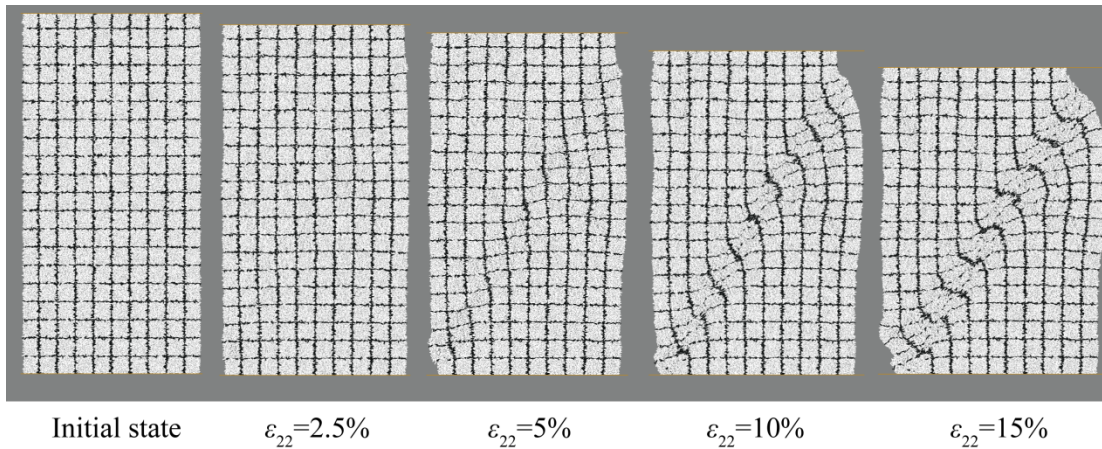


Figure 13 Deformation pattern of the biaxial compression specimen consisting of 45,000 elliptical.

In Figure 14, we track the evolutions of the vertical component (F_{22}) of each fabric tensor and the major principal axis angle $\bar{\theta}$. Because the initial values of these variables based on different microstructural quantities are very different from each other, we configure the plots in a way to emphasize the change of value from the initial values. When the axial strain is between 0 and 2%, the stress ratio monotonically increases and no shear-banding is apparent as seen in Figure 12 and Figure 13. In this stage of the deformation process, $F_{p,22}$ slightly decreases, indicating that the particles tend to further orient along the horizontal direction as a result of the vertical compression. The F_{22} components of the contact normal-

and void-based fabric tensors, on the other hand, both increase during this process. From the perspective of contact normals, more contacts in favor of bearing vertical stress has emerged, and the fabric anisotropy intensity increases since F_{22} is approximately the major principal component. The concurrent increase of $F_{n_{22}}$ and $F_{v_{22}}$ despite the decrease of $F_{p_{22}}$ resonates with the \mathbf{F}_n - \mathbf{F}_v correlation that we have discovered for non-elongated particles. Note that the F_{22} is the major principal component of \mathbf{F}_n but the minor principal component of \mathbf{F}_v . In this process, the fabric anisotropy of \mathbf{F}_n increases while that of \mathbf{F}_v decreases. In this particular case, because the anisotropy in the initial hydrostatic stress state is very strong, the magnitude of this change is not great enough to make $F_{v_{22}}$ the major principal component. However, if the inherent fabric anisotropy is weak, for example, when the particles are only slightly elongated, we can envision that the vertical compression loading might be able to increase $F_{v_{22}}$ to the extent that it becomes the major principal component. We also observe that in this stage of the deformation, the orientations of all three fabric tensors remain largely constant, which suggest that the symmetry of the simulated system is maintained.

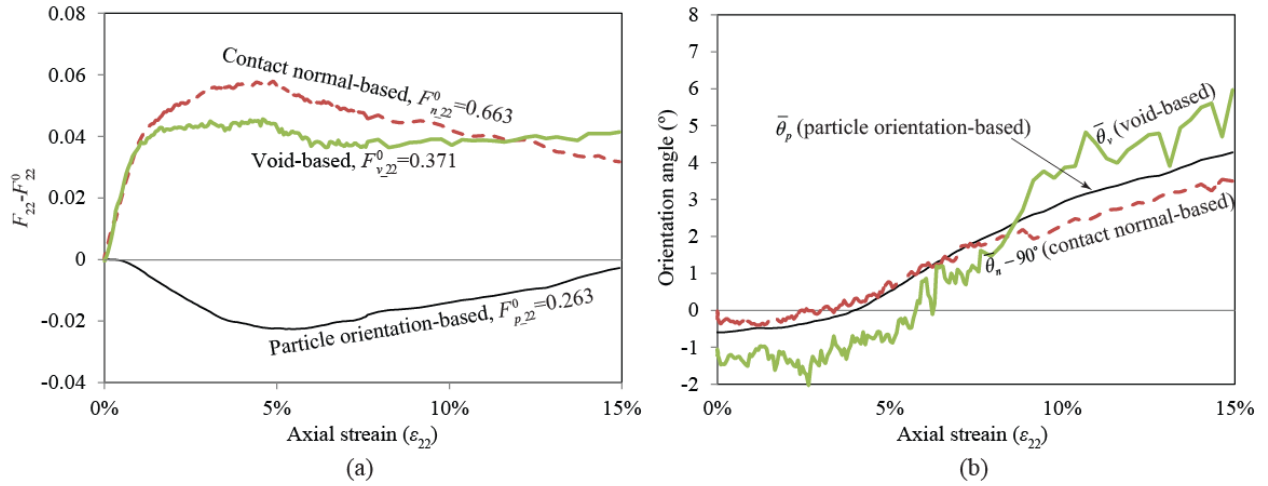


Figure 14 The evolutions of the vertical component (F_{22}) of each fabric tensor and the major principal axis angle $\bar{\theta}$.

When the axial strain increases beyond 5%, shear-banding dominates the deformation of the specimen. Although the stress ratio remains steady, $F_{p_{22}}$ (particle orientation-based) slowly increases. This phenomenon is related to the re-orientation of the particles in the shear band. According to our previous study (Fu and Dafalias, 2011b), the mean particle orientation in the shear band of this specimen is at approximately 40° counterclockwise from horizontal. The 22-component of F_p in the shear band should therefore be much greater than that at the initial state. This should be the main reason for the increasing trend of $F_{p_{22}}$ at axial strain greater than 5%. Because contact normal directions tend to be perpendicular to particle orientations, the increase $F_{p_{22}}$ is associated with a decrease of $F_{n_{22}}$. $F_{v_{22}}$ remains constant during this process, likely a consequence of the counteracting effects of increasing $F_{p_{22}}$ and decreasing $F_{n_{22}}$. As shown in Figure 14(b), all the three fabric tensors rotate counterclockwise at the same pace, which further supports the hypothesis that the evolution of the global fabric measurements mainly reflects the effects of particle rotation in the shear band from its initial state to the steady state.

Based on the very limited data presented, the following conclusions are tentatively drawn for granular materials composed of significantly elongated particles. In an isotropic stress state where inherent fabric

anisotropy applies while induced anisotropy (Oda et al., 1985; Guo and Zhao, 2013) does not play a significant role, the void-based fabric tensor (\mathbf{F}_v) is coaxial and highly correlated with the particle orientation-based fabric tensor (\mathbf{F}_p). In this state, intensity of contact normal-based fabric tensor (\mathbf{F}_n) is also positively correlated with that of the other fabric tensors, but the principal directions are perpendicular to those of the other two tensors. As the stress state of the specimen deviate from the isotropic stress state, increments of the fabric tensors are corresponding to the induced fabric anisotropy. The increment of \mathbf{F}_v normal components appear to be positively correlated to the corresponding components of both \mathbf{F}_n and \mathbf{F}_p . Because individual components of \mathbf{F}_n tend to be negatively correlated with the corresponding components of \mathbf{F}_p , the net effects on \mathbf{F}_v are dependent on the relatively magnitude of the change in \mathbf{F}_n and \mathbf{F}_p .

A multivariable regression between F_{p_22} , F_{n_22} , and F_{v_22} for this simulation yields

$$F_{v_22} = -0.68 + 1.18F_{p_22} + 1.12F_{n_22}$$

with a R^2 value of 0.83. The relationship between \mathbf{F}_v , \mathbf{F}_n , and \mathbf{F}_p is necessarily complicated, because \mathbf{F}_n and \mathbf{F}_p are highly correlated and not independent variables. Our investigation on this matter has not been comprehensive enough to definitely establish a universal correlation for elongated particles, but the regression results do support the observation made in the paragraph above.

6. Summary and concluding remarks

The current study explores the relationship between fabric tensors based on different classes of microstructural entities, namely particle orientations (\mathbf{F}_p), inter-particle contact normal directions (\mathbf{F}_n), and void shapes (\mathbf{F}_v). The void shapes based fabric tensor is motivated by, but is not identical, to the one introduced by Li and Li (2009), for reasons explained in the main text. For materials consisting of non-elongated particles, where only the two latter classes of fabric tensors apply, we discovered a simple and extremely strong correlation between \mathbf{F}_n and \mathbf{F}_v . This correlation holds for a great variety of conditions, including different densities, stress states, inter-particle friction angles, particle size distributions, and particle shapes. For materials composed of elongated particles, the situation is much more complicated. In an isotropic stress state where only inherent fabric anisotropy applies, \mathbf{F}_v is positively correlated with \mathbf{F}_p whereas \mathbf{F}_n is negatively correlated with \mathbf{F}_p . In terms of fabric anisotropy induced by deviatoric stress, the increment of \mathbf{F}_v normal components appears to be positively correlated with the increments of the corresponding components of both \mathbf{F}_p and \mathbf{F}_n , but \mathbf{F}_p and \mathbf{F}_n are to some extent negatively correlated. Although the study on elongated particles is not strongly conclusive, it does provide a few useful hints for further study in the future.

The main practical implication for the strong \mathbf{F}_n - \mathbf{F}_v correlation for non-elongated particle in regards to orientation and anisotropic intensity is that \mathbf{F}_v and \mathbf{F}_n for many materials can be largely used interchangeably for constitutive modeling purposes. This conclusion is especially useful when one of these two fabric tensors is required but the other one is easier to measure, or when we want to bridge existing studies or models based on different fabric tensors. Only when the physics associated with the contact normals and void shapes is considered, then the corresponding fabric tensor must be used to provide its own unique information. It should be noted that the current study is entirely based on 2D DEM simulation results. Given the extremely strong correlation in the 2D space, a similar relationship in 3D is

expected, although it is still to be proven. The very promising research direction pointed to by the 2D study will save a future 3D study a great amount of effort in exploring the vast variable space. Additionally, the relationship between the contact normal-based fabric tensor and void-based fabric tensors computed with scan-line type methods (Muhunthan and Chameau, 1997; Inglis and Pietruszczak, 2003; Ghedia and O’Sullivan, 2012) remains to be explored.

In the current study, the \mathbf{F}_n - \mathbf{F}_v correlation was established through empirical observation of simulation results. The extremely strong correlation might suggest that it may be possible to analytically derive the same relationship. However, there are two hints indicating otherwise: First, such a forward derivation is likely to be based on certain direct relationship between contact normal vectors and void vectors. We have shown in section 4.6 that the contact normal directions and void vectors directions can follow completely different distributions but the \mathbf{F}_n - \mathbf{F}_v correlation still holds. Second, the coefficient of the α_v - α_n correlation is dependent on the particle size distributions. This means that one has to condense particle size distribution features into one variable to be used the forward derivation, but there is not an apparent pathway for this treatment.

One last observation refers to the fact that DEM-based fabric tensors with no density related weight, such as the contact normal ones, are associated with a number of particles that have a defined solid volume (hence mass) with no reference to volume of the aggregate, thus, the tensors are not per-volume measures of anisotropic fabric. The latter property is important for a consistent dissipation-related definition of an internal variable in a continuum formulation. Therefore, such DEM-based tensors are excellent snap-shots of fabric anisotropy, but if their evolution is to be related to that of a fabric tensor that enters a continuum theory, they must be normalized by specific volume so that they become a per-volume measure. More details can be found in Li and Dafalias (2014).

Acknowledgments

Pengcheng Fu’s work in this paper was partly performed under the auspices of the U.S. Department of Energy by Lawrence Livermore National Laboratory under Contract DE-AC52-07NA27344. This document has been released with a release number: LLNL-JRNL-xxxxxx by LLNL. The research leading to these results has received funding from the European Research Council under the European Union's Seventh Framework Program FP7-ERC-IDEAS Advanced Grant Agreement n° 290963 (SOMEF), and partial support by NSF project CMMI-1162096.

References

- Alshibli, K., Cil, M.B., Kenesei, P. and Lienert, U., 2013. Strain tensor determination of compressed individual silica sand particles using high-energy synchrotron diffraction. *Granular Matter*, DOI: 10.1007/s10035-013-0424-x.
- Andò, E., Hall, S.A., Viggiani, G., Desrues, J., Bésuelle, P., 2011. Grain-scale experimental investigation of localised deformation in sand: a discrete particle tracking approach. *Acta Geotech.*, 7(1), 1–13.

- Berkowitz, B., Ewing, R.P., 1998. Percolation theory and network modeling applications in soil physics. *Surv. Geophys.*, 19(1), 23–72.
- Cowin, S., 1985. The relationship between the elasticity tensor and the fabric tensor. *Mech. Mater.*, 4, 137–147.
- Cundall, P.A., Strack, O.D.L., 1979. A discrete numerical model for granular assemblies. *Géotechnique*, 29(1), 47–65.
- Curray, J., 1956. The analysis of two-dimensional orientation data. *J. Geol.*, 64(2), 117–131.
- Dafalias, Y.F., Manzari, M.T., 2004. Simple plasticity sand model accounting for fabric change effects. *J. Eng. Mech.*, 130(6), 622–634.
- Dafalias, Y.F., Papadimitriou, A.G., Li, X.S., 2004. Sand plasticity model accounting for inherent fabric anisotropy. *J. Eng. Mech.*, 130(11), 1319–1333.
- Friedman, G.M., 1965. Terminology of crystallization textures and fabrics in sedimentary rocks. *J. Sediment. Res.*, 35, 643–655.
- Fu, P., Dafalias, Y.F., 2011a. Fabric evolution within shear bands of granular materials and its relation to critical state theory. *Int. J. Numer. Anal. Methods Geomech.*, 35(18), 1918–1948.
- Fu, P., Dafalias, Y.F., 2011b. Study of anisotropic shear strength of granular materials using DEM simulation. *Int. J. Numer. Anal. Methods Geomech.*, 35(10), 1098–1126.
- Fu, P., Walton, O.R., Harvey, J.T., 2012. Polyarc discrete element for efficiently simulating arbitrarily shaped 2D particles. *Int. J. Numer. Methods Eng.*, 89(5), 599–617.
- Fu, P., Dafalias, Y.F., 2012. Quantification of large and localized deformation in granular materials. *Int. J. Solids Struct.*, 49(13), 1741–1752.
- Ghedia, R., O’Sullivan, C., 2012. Quantifying void fabric using a scan-line approach. *Comput. Geotech.*, 41, 1–12.
- Gipson, M., 1965. Application of the electron microscope to the study of particle orientation and fissility in shale. *J. Sediment. Res.*, 35(2), 408–414.
- Guo, N., Zhao, J., 2013. The signature of shear-induced anisotropy in granular media. *Comput. Geotech.*, 47, 1–15.
- Hall, S.A., Bornert, M., Desrues, J., Pannier, Y., Lenoir, N., Viggiani, G., B  uelle, P., 2010. Discrete and continuum analysis of localised deformation in sand using X-ray CT and volumetric digital image correlation. *G  otechnique*, 60(5), 315–322.
- Harrigan, T.P., Mann, R.W., 1984. Characterization of microstructural anisotropy in orthotropic materials using a second rank tensor. *J. Mater. Sci.*, 19(3), 761–767.

- Hight, D.W., Symes, M.J., Gens, A., 1983. The development of a new hollow cylinder apparatus for investigating the effects of principal stress rotation in soils. *Géotechnique*, 33(4), 355–383.
- Inglis, D., Pietruszczak, S., 2003. Characterization of anisotropy in porous media by means of linear intercept measurements. *Int. J. Solids Struct.*, 40(5), 1243–1264.
- Konishi, J., Naruse, F., 1988. A note on fabric in terms of voids. *Micromechanics of Granular Materials, Proc., U.S. – Japan Seminar on the Micromechanics of Granular Materials*, M. Satake and J. T. Jenkins, eds., Elsevier, Amsterdam, Sendai-Zao, Japan, 39–46.
- Kuhn, M.R., 1999. Structured deformation in granular materials. *Mech. Mater.*, 31(6), 407–429.
- Laird, M.G., 1970. Vertical sheet structures; a new indicator of sedimentary fabric. *J. Sediment. Res.*, 40(1), 428–434.
- Li, X. and Li, X. S., 2009. Micro-macro quantification of the internal structure of granular materials. *J. Eng. Mech.*, 135(7), 641-656.
- Li, X., Yu, H.S., Li, X.S., 2009. Macro–micro relations in granular mechanics. *Int. J. Solids Struct*, 46(25-26), 4331–4341.
- Li, X.S., Dafalias, Y.F., 2012. Anisotropic critical state theory: role of fabric. *J. Eng. Mech.*, 138(3), 263–275.
- Li, X.S., Dafalias, Y.F., 2014. Thermodynamically Consistent Fabric Tensor Definition from DEM to Continuum. *Geomechanics from Micro to Macro IS-Cambridge*, K.Soga, ed., in preparation, Cambridge, U.K., 1-3 September 2014.
- Mitchell, J.K., Soga, K., 2005. *Fundamentals of Soil Behaviors*, third ed. John Wiley & Sons, Hoboken, New Jersey.
- Mollon, G., Zhao, J., 2012. Fourier–Voronoi-based generation of realistic samples for discrete modelling of granular materials. *Granular Matter*, 14(5), 621–638.
- Muhunthan, B., Chameau, J.L., 1997. Void fabric tensor and ultimate state surface of soils. *J. Geotech. Geoenviron. Eng.*, 123(2), 173–181.
- Oda, M., 1972a. The mechanism of fabric changes during compressional deformation of sand. *Soils and Foundations*, 12(2), 1–18.
- Oda, M., 1972b. Deformation mechanism of sand in triaxial compression tests. *Soils and Foundations*, 12(4), 45–63.
- Oda, M., 1982. Fabric tensor for discontinuous geological materials. *Soils and Foundations*, 22(4), 96–108.
- Oda, M., Nemat-Nasser, S., Konishi, J., 1985. Stress-induced anisotropy in granular masses. *Soils and Foundations*, 25(3), 85–97.

Rothenburg, L., Bathurst, R.J., 1992. Micromechanical features of granular assemblies with planar elliptical particles. *Géotechnique*, 42(1), 79–95.

Satake, M., 1982. Fabric tensor in granular materials. P. A. Vermeer and H. J. Luger, eds. In: *Deformation and Failure of Granular Materials*. Delft, 63–68.

Stallebrass, S., Baudet, B., 2004. A constitutive model for structured clays. *Géotechnique*, 54(4), 269–278.

Tong, Z. X., Zhang, J. M., Yu, Y. L., Zhang, G., 2010. Drained deformation behavior of anisotropic sands during cyclic rotation of principal stress axes. *J. Geotech. Geoenviron. Eng.*, 136(11), 1509–1518.

Yang, Z.X., Li X.S., Yang J., 2008. Quantifying and modelling fabric anisotropy of granular soils. *Geotechnique*, 58(4), 237-248.